J Biomol NMR (2008) 41:55–60
DOI 10.1007/s10858-008-9236-4

NMR STRUCTURE NOTE

Solution structure of wild-type human matrix metalloproteinase 12 (MMP-12) in complex with a tight-binding inhibitor

Michelle A. Markus · Brian Dwyer · Scott Wolfrom · Jianchang Li · Wei Li · Karl Malakian · James Wilhelm · Désirée H. H. Tsao

Received: 2 April 2008 / Accepted: 4 April 2008 / Published online: 19 April 2008

Abbreviations

3D	Three dimensional
4D	Four dimensional
DSV	*N*-(Dibenzo[*b,d*]thiophene-3-sulfonyl) valine
IPAP	In-phase antiphase (used for measuring H–N residual dipolar couplings)
MMP	Matrix metalloproteinase
NNGH	*n*-Isobutyl-*N*-[4-methoxyphenyl-sulfonyl]glycyl hydroxamic acid

Biological context

MMP-12 (macrophage elastase) is a member of a family of proteases that target proteins of the extracellular matrix. Matrix metalloproteinases (MMPs) influence tissue remodeling both in healthy growth and development and in the progression of pathological conditions such as arthritis and cancer. Members of the MMP family are specific for different components of the extracellular matrix and thus contribute to different disease states. They share a strongly conserved active site, including a catalytic zinc ion, coordinated by three conserved histidine side chains. The active site is contained within a groove along one face of the protein, the substrate binding cleft, that accommodates the protein chain to be cleaved. One wall of the substrate binding cleft is formed by the specificity loop, the loop between helix B and helix C. This loop varies in composition and length among members of the MMP family and contributes to the substrate specificity of the individual MMPs by forming much of the S1′ binding pocket.

MMP-12 was identified as the elastase activity produced by alveolar macrophages (Shapiro et al. 1993), although it shows activity against a range of basement membrane components, including fibronectin, laminin, entactin, chondroitan sulfate, and heparin sulfate (Gronski et al. 1997). Patients suffering from chronic obstructive pulmonary disease (COPD) show higher levels of MMP-12 in lung tissue and bronchoalveolar lavage (Molet et al. 2005). MMP-12 knockout mice are resistant to emphysema even when exposed to cigarette smoke (Hautamaki et al. 1997). These observations suggest that an MMP-12 inhibitor is a potentially disease-modifying treatment for COPD.

Previous MMP inhibitors have been plagued with musculoskeletal side effects (Wojtowicz-Praga 1998), presumably due to a lack of selectivity for the target enzyme. For many compounds, this lack of selectivity can be traced to a hydroxamate functionality, which provides affinity by chelating the catalytic zinc ion but prevents specificity, since all the enzymes in this family contain this zinc. To avoid these specificity issues, we have been interested in developing an inhibitor lacking the

M. A. Markus (✉) · B. Dwyer · S. Wolfrom · K. Malakian · J. Wilhelm · D. H. H. Tsao
Structural Biology and Computational Chemistry, Chemical and Screening Sciences, Wyeth Research, 87 CambridgePark Drive, Cambridge, MA 02140, USA
e-mail: mmarkus@wyeth.com

Present Address:
B. Dwyer
Novartis, 400 Technology Square, Cambridge, MA 02139, USA

Present Address:
S. Wolfrom
Protein Engineering and Chemistry, Adnexus Therapeutics, Waltham, MA 02453, USA

J. Li · W. Li
Medicinal Chemistry, Chemical and Screening Sciences, Wyeth Research, 87 CambridgePark Drive, Cambridge, MA 02140, USA

hydroxamate functionality. Here we report the solution structure of the catalytic domain of MMP-12 in complex with such an inhibitor, *N*-(dibenzo[*b,d*]thiophene-3-sulfonyl) valine (DSV), shown below:

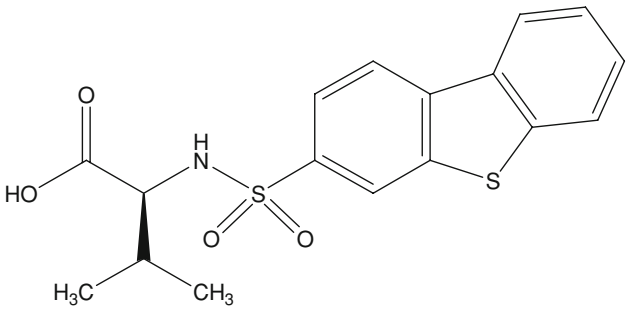

Although there are 18 entries in the Protein Data Bank for MMP-12, this inhibitor is unique among the complexes available. In contrast to the two previously published NMR structures for MMP-12 (Bertini et al. 2005; Bhaskaran et al. 2007), we use the wild type protein sequence to be as true as possible to the pharmacologically relevant species.

Methods and results

The protein expression, purification, and assignments have been described in the supplementary material to Markus et al. (2005). Briefly, the wild-type *Homo sapiens* sequence of the catalytic domain of MMP-12, corresponding to residues 100–263 of the full-length protein (18.3 kDa and 165 residues including the initiator methionine), was cloned into plasmid pET21a (Novagen) and expressed in *E. coli* strain BL21(DE3). The protein is recovered from the cell pellet by solubilizing with urea, purified on a Q sepharose column, and then refolded by gradually dialyzing away the urea. Final purification steps include affinity chromatography and gel filtration. Uniformly ^{15}N labeled, ^{15}N ^{13}C labeled, and 10% ^{13}C labeled samples including the DSV inhibitor were prepared. The buffer for structural studies includes 50 mM deuterated MES, 100 mM NaCl, 20 mM $CaCl_2$, 50 μM $ZnCl_2$, and 200 μM sodium azide, at pH 6.0. Backbone ^{15}N assignments are 96% complete; C_α assignments are 99% complete. Side chain assignments are complete for 121 of 165 residues.

Spectra were recorded at 25°C on Bruker Avance spectrometers. Most spectra were recorded at 600 MHz on instruments equipped with triple resonance, single axis gradient cryoprobes. An ^{15}N HSQC and two NOESY spectra were recorded on an instrument operating at 800 MHz with a triple resonance, triple axis gradient room temperature probe. These two NOESY spectra were 3D ^{15}N separated spectra, one with ^{1}H evolution in the remaining indirect dimension, the other with ^{13}C evolution (to give information equivalent to a 4D experiment), both with a mixing time of 80 ms. For additional NOE-based restraints, another 3D ^{15}N separated NOESY was recorded at 600 MHz with a mixing time of 140 ms. Three 3D carbon-separated NOESY spectra were analyzed to obtain restraints for structure calculations, with mixing times of 80, 100, and 120 ms. Spectra were processed using NMRPipe (Delaglio et al. 1995) and analyzed using PIPP and STAPP (Garrett et al. 1991). NOESY intensities were calibrated by analyzing intensities for crosspeaks corresponding to known distances in elements of regular secondary structure. Strips from the 3D ^{15}N separated NOESY acquired at 800 MHz are shown in Fig. 1a.

$^{3}J_{HNH\alpha}$ was measured using the HNHA experiment. Based on these coupling constants, 58 ϕ angles were restrained to the range $-100°$ to $-20°$ ($^{3}J_{HNH\alpha} < 5.5$ Hz) and 12 ϕ angles were restrained to $-160°$ to $-80°$ ($^{3}J_{HNH\alpha} > 8.0$ Hz). Additional ϕ restraints and ψ restraints were derived from the chemical shifts using TALOS (Cornilescu et al. 1999). Based on the HNHB and double quantum HACAHB experiments, β methylenes for 41 residues were stereospecifically assigned and χ_1 angles for 65 residues were restrained. Stereospecific assignments for the prochiral methyl groups of nine out of nine valines and nine out of nine leucines were determined from the pattern of splittings in a ^{13}C HSQC experiment recorded on a 10% ^{13}C enriched sample. Hydrogen bond restraints were included for backbone amides protected from exchange in $^{2}H_2O$ with obvious hydrogen bonding partners, based on preliminary structure calculations. Distance restraints were also included for side chains chelating the structural and catalytic zinc ions, based on observations from crystal structures of MMP-12 and MMP-13.

Structure determination with the restraints described above yielded structures with disorder in the loops, including the specificity loop, which is of special interest. To obtain additional restraints for structure calculations, residual dipolar couplings were measured in two media, a compressed 5% acrylamide gel (Ishii et al. 2001) and 4% alkylated polyethylene glycol (PEG)/hexanol (Rückert and Otting 2000). The following couplings were measured (with the experiment in parentheses): $^{1}D_{NH}$ (^{15}N IPAP (Ottiger et al. 1998)), $^{1}D_{NC'}$ (^{15}N HSQC, no C′ decoupling), $^{2}D_{HNC'}$ (^{15}N HSQC, no C′ decoupling), $^{1}D_{C\alpha C'}$ (HNCO, no Cα decoupling during C′ evolution), and $^{1}D_{H\alpha C\alpha}$ (HACA(CO)NH, no Hα decoupling during Cα evolution). The 3D experiments (HNCO, HACA(CO)NH) had relatively low sensitivity for MMP-12 and gave only a few couplings. The axial and rhombic coefficients for the molecular alignment tensor for each medium were fit by Powell minimization of a target function based on the difference between measured and calculated couplings (Tjandra and Bax 1997). A region of the ^{15}N IPAP experiment used to measure $^{1}D_{NH}$ in 4% alkylated PEG/hexanol is shown in Fig. 1b.

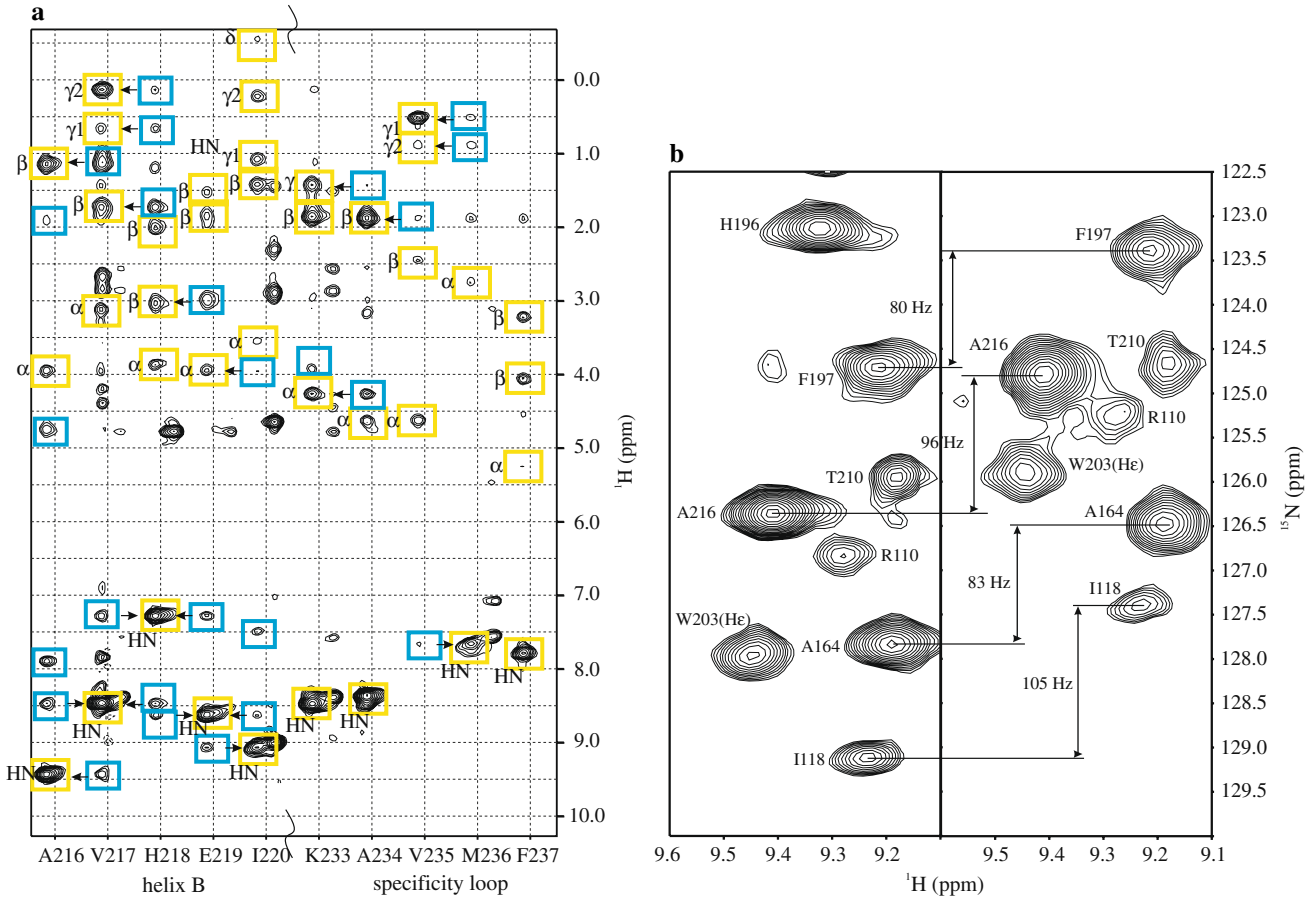

Fig. 1 (**a**) Strips from the ^{15}N separated NOESY acquired at 800 MHz. Strips on the left are from helix B; strips on the right are from the specificity loop. Peaks outlined in yellow are intraresidue peaks labelled with their source atoms. Peaks outlined in blue are sequential peaks. Note that while there are some strong intraresidue peaks in the specificity loop, the sequential peaks are fewer and weaker. (**b**) Regions of the ^{15}N IPAP spectrum used to determine $^1D_{NH}$ for a sample of ^{13}C ^{15}N MMP-12 in 4% alkylated PEG/hexanol. The difference spectrum is shown on the left; the sum spectrum is on the right. Peaks are labelled with the amino acid type and sequence position for the corresponding amide group. Note that for W203, the peak arises for the side chain. Some examples of splittings are labelled. Note that the observed splitting in this experiment is $^1D_{NH}$ plus $^1J_{NH}$ (typically about 93 Hz)

Intermolecular NOEs between the labeled protein and the unlabelled inhibitor were recorded with two isotope filtered 3D ^{13}C HMQC NOESY experiments (Lee et al. 1994) with mixing times of 100 and 120 ms. Peak intensities were used to set the reference distances for the corresponding distance restraints.

Structures were calculated using Xplor-NIH (Schwieters et al. 2003), version 2.11.0. Structures based on distance restraints and dihedral angle restraints were calculated with the distance geometry/simulated annealing protocol. The structure with the lowest X-PLOR energy was selected as the starting point for further simulated annealing calculations including restraints for the residual dipolar couplings. The restraints for the structure calculations and the resulting statistics are summarized in Tables 1 and 2. The coordinates for the ensemble of 17 structures, refined with residual dipolar couplings, have been deposited in the PDB with ID: 2k2g. The figures depicting the macromolecular structures were created with PyMOL (DeLano Scientific LLC, Palo Alto, CA).

Discussion and conclusions

The ensemble of 17 structures, refined with residual dipolar couplings, is shown in Fig. 2. The core of the protein is well-defined by the NMR data (Fig. 2a, backbone RMSD 0.53 ± 0.07 Å, excluding loops, compared to 0.47 ± 0.08 Å without RDCs). However, the loops, including the specificity loop, are not (Fig. 2b, backbone RMSD increases to 0.96 ± 0.12 Å for all residues from 13 to 164). For the specificity loop, this can be traced to a lack of long range NOEs, as suggested in Fig. 1a. Additional information from the residual dipolar couplings does not establish the conformation of the specificity loop, despite the determination of 32 couplings over the approximately 20

Table 1 Summary of restraints for structure calculations for MMP-12

Distance restraints	
NOE-derived	
Intraresidue	533
Sequential	762
Short range ($1 < i - j \leq 4$)	424
Long range ($i - j > 4$)	772
Intermolecular	63
Total NOE restraints	2,554
Hydrogen bonds	30
Zinc ions	2
Zinc coordination restraints	18
Total of all distance restraints	2,699
Dihedral angle restraints	
ϕ	92
ψ	85
χ_1	63
Total of all dihedral angle restraints	240
RDCs	
Compressed acrylamide	
NH	101
Alkylated PEG/hexanol	
NH	86
NC′	66
H_NC'	70
CαC′	38
HαCα	3
Total RDC restraints	364

Table 2 Summary of statistics for structure calculations for MMP-12

RMSD from ideal geometry	
Bonds	0.00320 ± 0.00009 Å
Angles	0.476 ± 0.009°
Impropers	0.379 ± 0.012°
RMSD from experimental restraints	
NOEs	0.024 ± 0.001 Å
Dihedrals	0.482 ± 0.047°
RDCs	1.58 ± 0.05 Hz
Ramachandran statistics[a] (%)	
Most favored	74.5
Allowed	18.2
Generously allowed	5.8
Disallowed	1.5
RMSD from the mean structure (Å)	
Backbone (111–262)	0.96 ± 0.12
Heavy (111–262)	1.43 ± 0.17
Backbone (well-ordered structure[b])	0.53 ± 0.07
Heavy (well-ordered structure[b])	1.03 ± 0.10

The ensemble of 17 structures with no violations above 0.5 Å and 5° from a calculation of 100 are considered

[a] Ramachandran statistics were calculated with PROCHECK (version 3.5.4, Laskowski et al. 1993)

[b] The well-ordered structure generally corresponds to the elements of regular secondary structure and includes residues 111–120, 126–152, 157–164, 182–185, 194–200, and 210–224

residues (229–248) of the loop. This is because couplings are available for approximately every other residue in the loop, due to overlap, weak signals, and missing assignments. If the conformation of the loop were well-defined by the NOE data, the available RDC data would have been enough to establish its conformation. This demonstrates that the specificity loop for MMP-12 is flexible, even in the presence of a tight binding inhibitor, as previously suggested (Bertini et al. 2005).

The structure reveals a fold consisting of two long α-helices plus a shorter, less well defined helix at the C-terminus and a five stranded mixed β-sheet, with most strands parallel except the edge strand, which is antiparallel to the neighboring strands. This is the classic fold observed for the MMP catalytic domain. In fact, there are 18 previous structures in the Protein Data Bank for MMP-12, including two published solution structures [(1YCM with minimized average 1Z3J from Bertini et al. (2005) and 2POJ from Bhaskaran et al. (2007)]. Overall, the solution structures are similar, with pairwise RMSDs for the ensembles of 1.60 ± 0.10 Å (1YCM to the present work), 1.58 ± 0.07 Å (2POJ to the present work), and 1.22 ± 0.09 Å (1YCM to 2POJ). Subject to the choice of alignment, it seems that the turn between β-strands IV and V pulls away from the core of the domain in the present structure more than in the two previous solution structures. It is tempting to speculate that this is due to the binding of a larger inhibitor. (1YCM has NNGH bound, which has only a single aromatic ring, while 2POJ is unliganded.) However, there are additional differences between the structures including different protein sequences[1] and different buffer conditions.[2] To minimize the impact these differences have on the results presented here, we will focus on what the present structure reveals about inhibitor binding and the potential for designing specific inhibitors.

The inhibitor DSV binds in the S1′ pocket, with NOEs observed to the edge strand of the β-sheet (strand IV), helix B, and the specificity loop. The carboxylate functionality of DSV coordinates the catalytic zinc ion (Fig. 3a).

[1] The wild type human sequence (methionine plus F100 to G263) is used here, the F171D mutation (in the context of methionine plus G106 to G263) for 1YCM, and the E219A inactivating mutation (in the context of F100 to G263) for 2POJ.

[2] The respective buffer conditions are: here—50 mM deuterated MES, 20 mM $CaCl_2$, 50 μM $ZnCl_2$, 100 mM NaCl, 200 μM NaN_3, pH 6.0; 1YCM—10 mM deuterated Tris, 5 mM $CaCl_2$, 100 μM $ZnCl_2$, 300 mM NaCl, pH 7.2; 2POJ—20 mM imidazole, 10 mM $CaCl_2$, 20 mM $ZnCl_2$, pH 6.6.

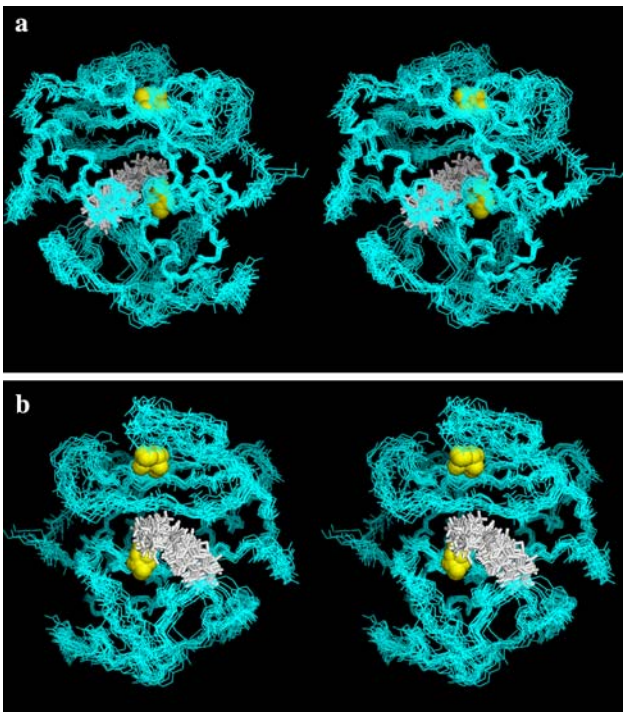

Fig. 2 Ensemble of 17 structures representing the structure of MMP-12 in solution, shown as stereo view. Only backbone atoms for residues 108–263 are shown because the N-terminal residues are disordered. The structural and catalytic zinc ions are shown as yellow spheres and the DSV ligands are shown as white sticks. (**a**) Elements of secondary structure in the core are well-defined, including helices A and B and some of the β-sheet. (**b**) The loops near the active site and along the substrate binding cleft are less well defined. The ensemble of structures has been rotated by 180° about the vertical axis of the plane compared to (**a**). The substrate binding cleft runs horizontally along the front of the molecule in this view, with the specificity loop at its lower edge. This is approximately the standard view for metalloproteinases.

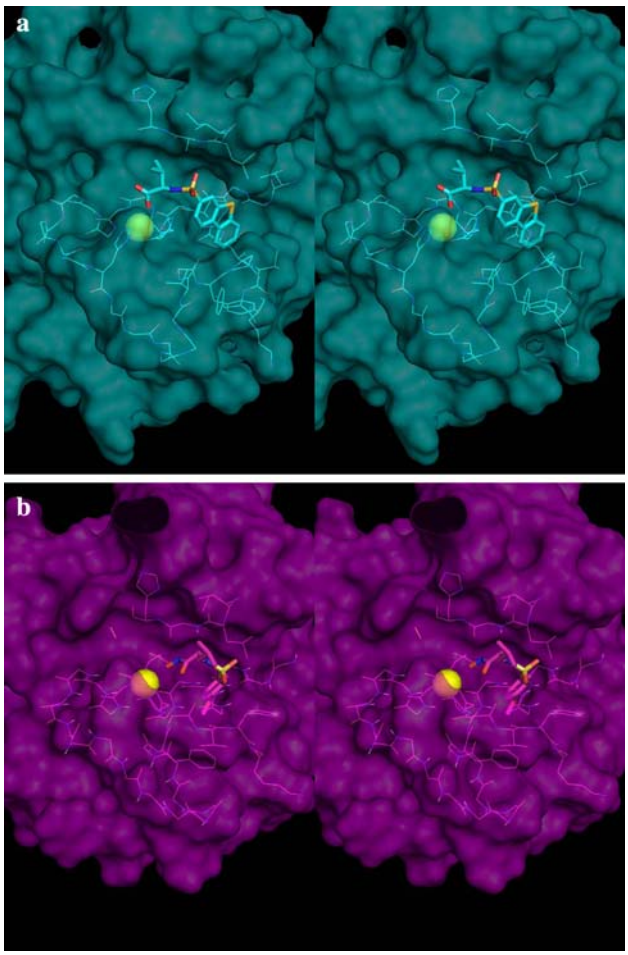

Fig. 3 Comparison of the inhibitor binding pockets for DSV and NNGH, based on one representative structure from each ensemble. For both examples, the protein surface is shown as a solid color. Backbone traces are shown for the regions of the protein which come closest to the ligands, including strand IV, helix B, and the specificity loop. The catalytic zinc ions are shown as yellow spheres. The inhibitors are shown as sticks: (**a**) the present structure, with DSV bound; (**b**) structure 1YCM (Bertini et al. 2005), with NNGH bound. Notice with the larger inhibitor (DSV) bound, the specificity loop is pushed down and the substrate binding cleft opens up

In 1YCM, NNGH also binds in the S1′ pocket, with NOEs observed to strand IV and the specificity loop (Fig. 3b). But the larger DSV ligand pushes the specificity loop away from the catalytic zinc ion to open up the substrate binding cleft more than observed with NNGH. The DSV ligand shows more NOEs to helix B, which forms the floor of the substrate binding cleft, and a unique NOE to V235, the residue adjacent to the methionine turn, compared to NNGH. Therefore, this structure demonstrates that protein flexibility readily accommodates the larger DSV ligand, mostly by reorienting the specificity loop. Note that although DSV, by its size alone, has more opportunity for energetically favorable interactions with the MMP-12 protein than NNGH, their binding affinities are similar (K_D of 7.5 nM for DSV and 10 nM for NNGH), possibly due to loss of entropy when the loop accommodates the larger ligand.

The structure presented here suggests a route to inhibitors specific for MMP-12. The residues involved in catalysis, including the histidine residues coordinating the catalytic zinc, the catalytic glutamate, and the active site methionine are highly conserved across the MMP family, making them poor targets to develop specificity. However, the specificity loop varies in both length and composition (Bode et al. 1999). The rearrangements observed to accommodate DSV suggest that larger inhibitors that are readily accommodated by MMP-12 will not be as readily accommodated by MMPs with shorter loops, providing first-order selectivity. To develop further selectivity using structure-based drug design (Kuntz 1992), it may be possible to target specific residues unique to the MMP-12 specificity loop. Given the adaptability demonstrated here for key loops near the substrate binding cleft, rational drug design targetting MMP-12 will need to incorporate protein flexibility as well as ligand flexibility.

Acknowledgements We thank Charles Schwieters for assistance with X-PLOR calculations. We thank Ad Bax for pulse sequences and advice on spectroscopy.

References

Bertini I, Calderone V, Cosenza M, Fragai M, Lee Y-M, Luchinat C, Mangani S, Terni B, Turano P (2005) Conformational variability of matrix metalloproteinases: beyond a single 3D structure. Proc Natl Acad Sci USA 102:5334–5339

Bhaskaran R, Palmier MO, Bagegni NA, Liang X, Van Doren SR (2007) Solution structure of inhibitor-free human metalloelastase (MMP-12) indicates an internal conformational adjustment. J Mol Biol 374:1333–1344

Bode W, Fernandez-Catalan C, Tschesche H, Grams F, Nagase H, Maskos K (1999) Structural properties of matrix metalloproteinases. Cell Mol Life Sci 55:639–652

Cornilescu G, Delaglio F, Bax A (1999) Protein backbone angle restraints from searching a database for chemical shift and sequence homology. J Biomol NMR 13:289–302

Delaglio F, Grzesiek S, Vuister GW, Zhu G, Pfeifer J, Bax A (1995) NMRPipe: a multidimensional spectral processing system based on UNIX pipes. J Biomol NMR 6:277–293

Garrett DS, Powers R, Gronenborn AM, Clore GM (1991) A common sense approach to peak picking in two-, three-, and four-dimensional spectra using automatic computer analysis of contour diagrams. J Magn Reson 95:214–220

Gronski TJ, Martin RL, Kobayashi DK, Walsh BC, Holman MC, Huber M, Van Wart HE, Shapiro SD (1997) Hydrolysis of a broad spectrum of extracellular matrix proteins by human macrophage elastase. J Biol Chem 272:12189–12194

Hautamaki RD, Kobayashi DK, Senior RM, Shapiro SD (1997) Requirement for macrophage elastase for cigarette smoke-induced emphysema in mice. Science 277:2002–2004

Ishii Y, Markus MA, Tycko R (2001) Controlling residual dipolar couplings in high-resolution NMR of proteins by strain induced alignment in a gel. J Biomol NMR 21:141–151

Kuntz ID (1992) Structure-based strategies for drug design and discovery. Science 257:1078–1082

Laskowski RA, MacArthur MW, Moss DS, Thornton JM (1993) PROCHECK: a program to check the stereochemical quality of protein structures. J Appl Cryst 26:283–291

Lee W, Revington MJ, Arrowsmith C, Kay LE (1994) A pulsed field gradient isotope-filtered 3D ^{13}C HMQC-NOESY experiment for extracting intermolecular NOE contacts in molecular complexes. FEBS Lett 350:87–90

Markus MA, Dwyer B, Wolfrom S, Li J, Li W, Malakian K, Wilhelm J, Tsao DHH (2005) ^{1}H, ^{13}C, and ^{15}N assignments of MMP-12, a key protease implicated in lung tissue remodeling. J Biomol NMR 31:260

Molet S, Belleguic C, Lena H, Germain N, Bertrand CP, Shapiro SD, Planquois J-M, Delaval P, Lagente V (2005) Increase in macrophage elastase (MMP-12) in lungs from patients with chronic obstructive pulmonary disease. Inflamm Res 54: 31–36

Ottiger M, Delaglio F, Bax A (1998) Measurement of *J* and dipolar couplings from simplified two-dimensional NMR spectra. J Magn Reson 131:373–378

Rückert M, Otting G (2000) Alignment of biological macromolecules in novel nonionic liquid crystalline media for NMR experiments. J Am Chem Soc 122:7793–7797

Schwieters CD, Kuszewski JJ, Tjandra N, Clore GM (2003) The Xplor-NIH NMR molecular structure determination package. J Magn Reson 160:65–73

Shapiro SD, Kobayashi DK, Ley TJ (1993) Cloning and characterization of a unique elastolytic metalloproteinase produced by human alveolar macrophages. J Biol Chem 268:23824–23829

Tjandra N, Bax A (1997) Direct measurement of distances and angles in biomolecules by NMR in a dilute liquid crystalline medium. Science 278:1111–1114

Wojtowicz-Praga S, Torri J, Johnson M, Steen V, Marshall J, Ness E, Dickson R, Sale M, Rasmussen HS, Chiodo TA, Hawkins MJ (1998) Phase I trial of Marimastat, a novel matrix metalloproteinase inhibitor, administered orally to patients with advanced lung cancer. J Clin Oncol 16:2150–2156